The Journal of Chemical Physics

Microphase separation and aggregate self-assembly in brushes of oppositely charged polyelectrolytes triggered by ion pairing

Cite as: J. Chem. Phys. **153**, 144903 (2020); https://doi.org/10.1063/5.0020779
Submitted: 03 July 2020 . Accepted: 21 September 2020 . Published Online: 12 October 2020

Gabriel Debais, and Mario Tagliazucchi

The Journal of Chemical Physics ARTICLE scitation.org/journal/jcp

Microphase separation and aggregate self-assembly in brushes of oppositely charged polyelectrolytes triggered by ion pairing

Cite as: J. Chem. Phys. 153, 144903 (2020); doi: 10.1063/5.0020779
Submitted: 3 July 2020 • Accepted: 21 September 2020 •
Published Online: 12 October 2020

Gabriel Debais and Mario Tagliazucchi[a)]

AFFILIATIONS

Instituto de Química Física de los Materiales, Medio Ambiente y Energía and Departamento de Química Inorgánica Analítica y Química Física, Universidad de Buenos Aires, Facultad de Ciencias Exactas y Naturales, Ciudad Universitaria, Pabellón 2, Ciudad Autónoma de Buenos Aires C1428EHA, Argentina

[a)]**Author to whom correspondence should be addressed:** mario@qi.fcen.uba.ar.
URL: http://www.inquimae.fcen.uba.ar/softmaterials/

ABSTRACT

This work applies a molecular theory to study the formation of lateral self-assembled aggregates in mixed brushes composed of polyanion and polycation chains. In order to overcome the well-known limitations of mean-field electrostatics to capture polyelectrolyte complexation, the formation of ion pairs between anionic and cationic groups in the polyelectrolytes is explicitly modeled in our theory as an association reaction. This feature is essential to capture the microphase separation of the mixed brush and the formation of lateral aggregates triggered by polyelectrolyte complexation. The effects of solution pH and ionic strength, surface coverage, and chain length on the morphology of the mixed brush are systematically explored. It is shown that increasing salt concentration leads to the rupture of polyelectrolyte complexes and the stabilization of the homogeneous, non-aggregated brush, providing that the formation of ion pairs between the polyelectrolytes and the salt ions in solution is explicitly accounted for by the theory. The inclusion of ion-pairing association reactions between oppositely charged polyelectrolytes within a mean-field description of electrostatics emerges from this work as a useful and simple theoretical approach to capture the formation of polyelectrolyte complexes and their responsiveness to solution ionic strength and pH.

I. INTRODUCTION

Polyanions and polycations mixed in solution are known to form interpolyelectrolyte complexes stabilized by ion pairs between the charged groups in the polyelectrolyte chains.[1–4] The formation of these ion pairs results in the expulsion of small counterions that are condensed on the polyelectrolytes. This entropic process—known as counterion release—is now recognized to be a main driving force behind polyelectrolyte complexation.[2,3,5–8] The formation of interpolyelectrolyte complexes in solution usually results in the separation of a polyelectrolyte-rich solid precipitate or liquid coacervate and a polyelectrolyte-poor solution.[1,2] On the other hand, a mixture of polycations and polyanions end-grafted to a surface, i.e., a mixed polyelectrolyte brush,[9–14] is also expected to form interpolymer complexes on the surface, but it cannot macroscopically phase-separate because of the constraints introduced by grafting. In this work, we theoretically study whether the complexion of oppositely charged polyions in a mixed polyelectrolyte brush can lead to the formation of lateral aggregates via a microphase-separation process.[15,16]

Polyelectrolyte complexation is a key phenomenon for different technologies and applications. Protein/polysaccharide complexes and coacervates have important applications as emulsifiers, viscosity enhancers, and platforms for nano/microencapsulation.[17,18] Polyelectrolyte complexation is also likely to be a dominant force in the formation of biologically relevant membraneless organelles[19–21] and underwater adhesives.[22] The formation of polyelectrolyte complexes at interfaces serves as the basis of the layer-by-layer method for the

fabrication of ultrathin polyelectrolyte films.[4,23] Polyelectrolyte complexation can be relevant in the field of polyelectrolyte brushes, for example, when two opposing surfaces bearing a polycation and a polyanion brush, respectively, are brought into contact.[24–26] Alternatively, the polycation and polyanion chains may be grafted onto the same surface and form a mixed polyelectrolyte brush.[9–11,13,14,27] The latter type of mixed brush has been much less studied than single-component polyelectrolyte brushes or mixed neutral-polymer brushes,[28] but its amphoteric properties made it very appealing for switchable surfaces.[9,10,14,27]

Houbenov *et al.* reported the first example of a mixed polyanionic/polycationic brush.[9] Both the polycation [poly(2-vinylpyridine) (P2VP)] and the polyanion [poly(acrylic acid) (PAA)] used in the study were weak polyelectrolytes, which allowed the control of the morphology of the system by changing the pH. A minimum thickness (most compact state) was obtained between pHs 4 and 8, when both polyelectrolytes were partially ionized.[9] Drechsler *et al.* studied the morphology of this system using *in situ* AFM imaging as a function of the solution pH and ionic strength.[13] These authors observed ripple-like structures at low ionic strengths (1 mM), which were ascribed to aggregates (bundles) of interacting PAA and P2VP chains. These ripple structures softened at high ionic strengths (1M), which is in agreement with the expected destabilizing effect of added salt on interpolyelectrolyte complexes.[1,3,24,29–31]

The technological and biological relevance of interpolyelectrolyte complexes has motivated theoretical models and simulations to rationalize their behavior. Mixed polyelectrolyte brushes were theoretically studied by lattice theory[32] and a molecular theory.[33] In both cases, the theory predicted a polymer-density profile that is highly heterogeneous in the direction normal to the surface, which indicates a coexistence of stretched and collapsed chains within the brush. However, these theoretical works did not predict the possibility of lateral aggregates (i.e., the formation of inhomogeneities in the plane of the substrate), and, therefore, they cannot explain the nanomorphologies observed by AFM by Drechsler *et al.*[13] We believe that a main limitation of previous works to predict lateral phase separation resides in the mean-field treatment of electrostatic interactions. Mean-field electrostatics neglects the correlations between the polycation and polyanion that are important to properly describe the formation of ion pairs and, ultimately, the assembly of interpolyelectrolyte complexes. Theoretical tools to model polyelectrolyte complexes in solution beyond the mean-field level[34] include the random phase approximation,[35–38] field theoretic approaches,[39,40] and the PRISM theory.[41] On the other hand, the theoretical description of polyelectrolyte complexation on interfaces has received much less attention than that in solution.

In this work, we introduce a molecular theory that captures the formation of polyelectrolyte complexes by explicitly considering the formation of ion pairs between the segments of the oppositely charged polyelectrolytes. Borrowing previous ideas from the fields of layer-by-layer self-assembly[42,43] and polyelectrolyte complexation in solution,[2,31,36] we model the formation of these ion pairs as an association chemical reaction. We apply the theory to study the structure of mixed polyanion/polycation brushes and to systematically investigate the effect of the polyelectrolyte surface coverage and chain length, and the solution pH and the ionic strength on the onset conditions for microphase separation. We show that the formation of lateral aggregates is not predicted to occur in the absence of the ion-pairing reaction and ascribe this observation to the fact that mean-field electrostatic interactions by themselves cannot properly describe polyelectrolyte complexation. Moreover, we show that in order to capture the well-known destabilizing effect of added salt on polyelectrolyte complexes, it is also necessary to include in the theory the association of small salt ions with the charges in the polyelectrolyte, which we also model as association reactions.

II. THEORETICAL APPROACH

A. Formation of ion pairs and coupled chemical equilibria

Figure 1 shows a scheme of the system under consideration: a mixed brush of a weak polyacid (polyanion) and a weak polybase (polycation) in a solution containing protons, hydroxyl ions, salt anions (e.g., Cl^-), and cations (e.g., Na^+). As shown in Fig. 1, each segment in the polyions can participate in three different association reactions:

(i) Association with protons or hydroxyl ions in solution (i.e., acid–base reactions). These reactions include the acid–base equilibria of the dissociation of acid groups in the polyacid chains,

$$\text{Pol–AH} \rightleftharpoons \text{Pol–A}^- + \text{H}^+, \tag{1}$$

and of the base groups in the polybase,

$$\text{Pol–B} + \text{H}_2\text{O} \rightleftharpoons \text{Pol–BH}^+ + \text{OH}^-. \tag{2}$$

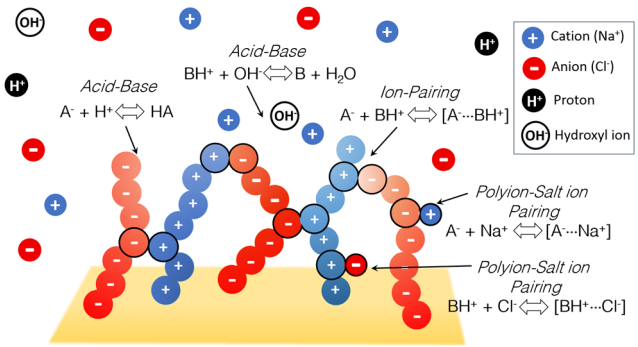

FIG. 1. We consider a mixed brush of a weak polyacid (polyanion) and a weak polybase (polycation) immersed in an aqueous solution of salt ions (anions and cations), protons, and hydroxyl ions. The polyelectrolyte chains are under good solvent conditions, i.e., there are no effective non-electrostatic attractive interactions between the polymer segments. The total surface density of grafting points is $\sigma = \sigma_A + \sigma_B$, and the length of the chains is N. The theory explicitly considers the formation of ion pairs between the acid and basic groups in the polyelectrolytes (polyion–polyion ion pairs), their corresponding acid–base reactions, and the formation of ions pairs between the anionic and cationic groups of the polyelectrolyte and free salt ions in solution (ion–polyion ion pairs).

(ii) Association between charged groups in the polyelectrolytes according to the reaction:

$$\text{Pol–A}^- + \text{Pol–BH}^+ \rightleftharpoons [\text{Pol–A}^-\text{Pol–BH}^+]. \quad (3)$$

The inclusion of the ion-pair formation between polyions in a molecular theory is a novel feature of the present work, which is inspired by previous ideas in the field of layer-by-layer films[42,43] and polyelectrolyte complexes in solution.[2,31,36] We demonstrate below that this feature enables the formation of aggregates in the mixed polyelectrolyte brushes. We will refer hereafter to the process described by Eq. (3) as the formation of polyion–polyion ion pairs to distinguish it from the ion–polyion ion pairs described in the next paragraph.

(iii) Association between the charged groups in the polyelectrolyte chains and free salt ions in solution (also referred to as counterion condensation[44]). We propose to model this process as an association chemical reaction.[31,36] The formation of ion pairs between the polyanion and a cation in solution is, thus, described by

$$\text{Pol–A}^- + \text{Na}^+ \rightleftharpoons \text{Pol–ANa}, \quad (4)$$

and the association of the polycation and an anion in solution is described by

$$\text{Pol–BH}^+ + \text{Cl}^- \rightleftharpoons \text{Pol–BHCl}. \quad (5)$$

We will refer hereafter to the ion pairs formed in Eqs. (4) and (5) as ion–polyion ion pairs.

B. Molecular theory for a brush of oppositely charged polyelectrolytes

In order to formulate the molecular theory for this system, we start by writing down an approximate Helmholtz free-energy functional, which has contributions from the translational entropy of the solvent and the ions ($-TS_{\text{Trans}}$), the internal free energy of these species associated with their standard chemical potential (F_{int}), the conformational entropy of the polyelectrolyte chains ($-TS_{\text{Conf}}$), the free energy related to chemical acid–base and ion-pairing equilibria (F_{Chem}), and the electrostatic contribution (F_{Elect}),

$$\beta F = -S_{Trans}/k_B + \beta F_{int} - S_{Conf}/k_B + \beta F_{Chem} + \beta F_{Elect}, \quad (6)$$

where k_B is Boltzmann's constant.

The term $-S_{\text{Trans}}/k_B$, accounting for the translational (mixing) free-energy of solvent molecules and ions, is given by

$$-S_{Trans}/k_B = \sum_{i=\text{H}^+,\text{OH}^-,\text{Na}^+,\text{Cl}^-,s} \int \rho_i(\mathbf{r})[\ln(\rho_i(\mathbf{r})v_s) - 1]d\mathbf{r}, \quad (7)$$

where i = H^+, OH^-, Na^+, Cl^-, *s* for protons, hydroxyl ions, salt cations, salt anions, and solvent molecules (water), respectively. $\rho_i(\mathbf{r})$ is the number density at position $\mathbf{r}$ and v_s molecular volume of the solvent. The next term is the internal free energy of mobile species,

$$\beta F_{int} = \sum_{i=\text{H}^+,\text{OH}^-,\text{Na}^+,\text{Cl}^-,s} \int \rho_i(\mathbf{r})\beta\mu_i^o d\mathbf{r}, \quad (8)$$

where μ^o_i is the standard chemical potential of species i.

The third term in Eq. (6) represents the conformational entropy of the polymers, which is given by

$$-S_{conf}/k_B = \sum_j^{N_A}\sum_{\alpha_A} P_A(\alpha_A, j)\ln(P_A(\alpha_A, j)) + \sum_j^{N_B}\sum_{\alpha_B} P_B(\alpha_B, j)\ln(P_B(\alpha_B, j)), \quad (9)$$

where the summations over *j* run over the total number of chains of each type. In this equation, $P_A(\alpha_A, j)$ is the probability of having the polyanion at the grafting point *j* in the conformation α_A and $P_B(\alpha_B, j)$ is defined analogously for the polybase.

The fourth term, βF_{chem}, includes all contributions to the free energy from the chemical reactions in the system. This term is given by

$$\beta F_{chem} = \int \langle n_A(\mathbf{r})\rangle \sum_{\substack{j=c,uc,\\ as,as\text{ - }ion}} f_j^A(\mathbf{r})\left(\ln(f_j^A(\mathbf{r})) + \beta\mu_j^{o,A}\right)d\mathbf{r} + \int \langle n_B(\mathbf{r})\rangle \sum_{\substack{j=c,uc,\\ as,as\text{ - }ion}} f_j^B(\mathbf{r})\left(\ln(f_j^B(\mathbf{r})) + \beta\mu_j^{o,B}\right)d\mathbf{r} - \int \langle n_A(\mathbf{r})\rangle f_{as}^A(\mathbf{r})\left(\ln\left(\langle n_A(\mathbf{r})\rangle f_{as}^A(\mathbf{r})v_{AB}\right) - 1\right)d\mathbf{r}. \quad (10)$$

The summation over *j* in the first and second terms of Eq. (10) includes all possible states of a segment in the polyelectrolyte chains: charged ("*c*," correspond to pol-A^- and pol-BH^+), uncharged ("*uc*," pol-AH and pol-B), associated ("*as*," correspond to the [pol-$A^-\cdots$pol-BH^+] complex) and associated with a salt ion ("*as-ion*," pol-ANa, and pol-BHCl). The expression in Eq. (10) results from the combination of different chemical equilibria considered in previous studies,[45–49] namely: (i) acid–base reactions,[47,50] (ii) polymer–polymer association,[48,49] and (iii) ion–polyion ion-pair formation.[45,51] In Eq. (10), $\mu^{o,i}_j$ and $f_j^i(\mathbf{r})$ denote the chemical potential and the fraction of monomers, respectively, of state *j* (*j* = *c*,*uc*,*as*,*as-ion*) for a segment of type *i* (*i* = A, B). v_{AB} is the volume of the [pol-$A^-\cdots$pol-BH^+] complex. We present a detailed derivation of Eq. (10) in the supplementary material.

It is important to remark that the fractions of segments in the different states are not independent, since their summation must fulfill

$$\sum_{\substack{j=c,uc,\\ as,as\text{ - }ion}} f_j^i(\mathbf{r}) = 1 \text{ for i = A, B.} \quad (11)$$

In Eq. (10), $\langle n_i(\mathbf{r})\rangle$ is the total concentration of monomers of type *i* (*i* = A, B) at position $\mathbf{r}$, which is given by

$$\langle n_i(\mathbf{r})\rangle = \sum_j^{N_i}\sum_{\alpha_i} P_i(\alpha_i, j)n_i(\mathbf{r}; \alpha_i, j), \quad (12)$$

where $n_i(\mathbf{r};\alpha_i, j)d\mathbf{r}$ is the number of polymer segments that a chain of type *i* (*i* = A, B) in conformation α_i and tethered to the grafting point *j* has in the element of volume between $\mathbf{r}$ and $\mathbf{r} + d\mathbf{r}$.

The last term in Eq. (6) is the electrostatic contribution to the free energy. Here, $\psi(\mathbf{r})$ is the electrostatic potential and ϵ is the dielectric permittivity,

$$\beta F_{elec} = \beta \int [\langle \rho_q(\mathbf{r})\rangle \psi(\mathbf{r}) - \frac{1}{2}\epsilon(\nabla\psi(\mathbf{r}))^2]d\mathbf{r}, \tag{13}$$

where the total charge density is

$$\langle \rho_q(\mathbf{r})\rangle = f_c^A(\mathbf{r}) q_A \langle n_A(\mathbf{r})\rangle + f_c^B(\mathbf{r}) q_B \langle n_B(\mathbf{r})\rangle + \sum_{i=\mathrm{H^+,OH^-,Na^+,Cl^-}} q_i \rho_i(\mathbf{r}), \tag{14}$$

where q_i is the charge of the species i. We remark that the electrostatic contribution in Eq. (13) does not account for the formation of ion pairs because of its mean-field nature. Therefore, we explicitly consider the formation of ion pairs in our theory in the F_{chem} term, as described above. Note also that the dielectric permittivity is assumed to be constant throughout the system. In a previous study, the lateral pressure of a single-component polyelectrolyte brush (which is the relevant quantity to study microphase separation, see below) was shown to be almost identical for position-independent and position-dependent dielectric functions (see Fig. 5 in Ref. 50).

It is important to note that the chemical potential of the ions in the system is fixed by their concentration in the bulk solution; therefore, the proper thermodynamic potential that describes the system is not the Helmholtz free energy (which considers fixed number of particles), but rather a potential that is grand-canonical for the ions and solvent and canonical for the polyelectrolyte chains. This potential is

$$\begin{aligned}\beta\omega = \beta F &- \sum_{i=\mathrm{Na^+,Cl^-,H^+,OH^-},s} \beta\mu_i \int \rho_i(\mathbf{r})d\mathbf{r} - \beta\mu_{\mathrm{H^+}} \int f_{uc}^A(\mathbf{r})\langle n_A(\mathbf{r})\rangle d\mathbf{r} \\ &- \beta\mu_{\mathrm{Na^+}} \int f_{as-ion}^A(\mathbf{r})\langle n_A(\mathbf{r})\rangle d\mathbf{r} - \beta\mu_{\mathrm{OH^-}} \int f_{uc}^B(\mathbf{r})\langle n_B(\mathbf{r})\rangle d\mathbf{r} \\ &- \beta\mu_{Cl^-} \int f_{as-ion}^B(\mathbf{r})\langle n_B(\mathbf{r})\rangle d\mathbf{r},\end{aligned} \tag{15}$$

where the third and fourth terms in the right-hand side account for the protons and salt cations associated with the polyacid and the fifth and sixth terms correspond to the hydroxyl ions and salt anions associated with the polybase.

So far, we have not discussed attractive and repulsive interactions in our theory besides the association processes modeled as chemical reactions. In previous studies for single-component polymer brushes under poor solvent conditions,[15,46,47,52,53] microphase separation resulted from the short-range effective van der Waals attractions between polymer segments (difference between segment–segment and segment-solvent attractions). In the present work, short-range van der Waals attractions were on purposely not included in the theory because we are interested in studying whether the formation of ion-pairs can trigger aggregate formation in mixed polyacid/polybase polymer brushes, even in a good solvent for both polyelectrolyte chains.

Repulsions in the theory are approximately treated as excluded-volume interactions using a packing constraint:

$$\langle \phi_A(\mathbf{r})\rangle + \langle \phi_B(\mathbf{r})\rangle + \sum_{i=\mathrm{H^+,OH^-,Na^+,Cl^-},s} \rho_i(\mathbf{r}) v_i = 1 \text{ at all } \mathbf{r}, \tag{16}$$

where v_i is the volume of species i and $\langle \phi_i(\mathbf{r})\rangle = \langle n_i(\mathbf{r})\rangle v_p$ is the volume fraction of segments of type i (i = A, B). The volume of a polymer segments is v_P and it is assumed to be the same for all four states of the segment and both types of polymers. Equation (16) models all repulsive interactions in the theory, with the exception of intrachain repulsions, which are exactly considered by excluding self-overlapping chain conformations.

There is a second constraint that enforces the stoichiometry of polyion–polyion ion pairs: at each $\mathbf{r}$, the number density of associated A-type and B-type segments must be the same,

$$\langle n_A(\mathbf{r})\rangle f_{as}^A(\mathbf{r}) = \langle n_B(\mathbf{r})\rangle f_{as}^B(\mathbf{r}). \tag{17}$$

A final constraint involves the normalization of the probability distribution functions for the chain conformations, $P_i(\alpha_A, j)$,

$$\sum_{\alpha_i} P_i(\alpha_i, j) = 1 \text{ for all } j \text{ and } i = \mathrm{A, B}. \tag{18}$$

The constraints in Eqs. (16)–(18) are enforced using Lagrange multipliers. Therefore, the equilibrium state of the system corresponds to an extreme of the following potential:

$$\begin{aligned}\mathcal{L} = \beta w + \beta \int \pi(\mathbf{r}) &\left(\langle \phi_A(\mathbf{r})\rangle + \langle \phi_B(\mathbf{r})\rangle + \sum_{i=s,\mathrm{Na^+,Cl^-,H^+,OH^-}} \rho_i(\mathbf{r}) v_i - 1 \right) d\mathbf{r} \\ &+ \int \lambda(\mathbf{r}) \left[\langle n_A(\mathbf{r})\rangle f_{as}^A(\mathbf{r}) - \langle n_B(\mathbf{r})\rangle f_{as}^B(\mathbf{r}) \right] d\mathbf{r} \\ &+ \sum_{i=A,B} \sum_{j}^{N_i} \xi_i(j) \left(\sum_{\alpha_i} P_i(\alpha_i, j) - 1 \right).\end{aligned} \tag{19}$$

The functional extrema of this potential with respect to the unknown functions in the theory, $\rho_i(\mathbf{r})$, $P_i(\alpha_i, j)$, $\psi(\mathbf{r})$, $f_c^i(\mathbf{r})$, $f_{uc}{}^i(\mathbf{r})$, $f_{as}{}^i(\mathbf{r})$, and $f_{as\text{-}ion}{}^i(\mathbf{r})$, lead to expressions for these quantities in equilibrium. For simplicity, we will describe the final expressions that are obtained after rearrangements and substitutions.

The extreme of $\mathcal{L}$ with respect to $P_i(\alpha_i, j)$ (for i = A, B) results in

$$\begin{aligned}P_i(\alpha_i, j) = \frac{1}{q_i(j)} \exp\Big[- \int n_i(\mathbf{r}; \alpha_i, j) \big(&\ln(f_c^i(\mathbf{r})) \\ &+ q_i \beta\psi(\mathbf{r}) + \beta v_p \pi(\mathbf{r}) \big) d\mathbf{r} \Big],\end{aligned} \tag{20}$$

where $q_i(j) = 1/\exp(1 + \xi_i(j))$ is a single-chain partition function. The expression in parentheses in Boltzmann's factor has contributions related to the electrostatic $[q_i\beta\psi(\mathbf{r})]$ and osmotic-pressure $[v_p\beta\pi(\mathbf{r})]$ interactions, in addition to the term $\ln[f^i{}_c(\mathbf{r})]$ that results from the fact that each segment can exist in four different chemical states. This last term is related to an entropic effect that arises from the chemical contribution to the free energy. As explained in Ref. 50, Boltzmann's factor in Eq. (20) can be written in terms of any of the four possible chemical states considered in the present theory. The factor $\ln[f^i{}_j(\mathbf{r})]$ (where j is the chosen state) appears in Boltzmann's factor as a result of that choice. In Eq. (20), Boltzmann's factor was written in terms of the charged state ($j = c$) and, for that reason, it contains the electrostatic contribution $q_i\beta\psi(\mathbf{r})$, which is the energy of interaction of a charged segment with the electrostatic potential ($q_i = -|e|$ and $|e|$ for acid and basic segments, respectively).

The density distribution of each mobile species, $i = s$, OH^-, H^+, Na^+, Cl^-, obtained from the corresponding functional derivatives of $\mathcal{L}$ are

$$\rho_i(\mathbf{r})v_i = \exp(-\beta(\mu_i^o - \mu_i(\mathbf{r}) + \pi(\mathbf{r})v_i + q_i\psi(\mathbf{r}))). \quad (21)$$

For the solvent (s), this expression is reduced to[50]

$$\rho_s(\mathbf{r})v_s = \exp(-\beta\pi(\mathbf{r})v_s). \quad (22)$$

It is possible to rewrite the expressions of the local densities $\rho_i(\mathbf{r})$ in terms of the concentrations in the bulk.[45,47,50]

The minimization of $\mathcal{L}$ with respect to the fractions $f^i{}_c(\mathbf{r})$, $f^i{}_{uc}(\mathbf{r})$, $f^i{}_{as}(\mathbf{r})$, and $f^i{}_{as\text{-}ion}(\mathbf{r})$ for i = A, B results in chemical equilibrium equations. For the acid–base dissociation reaction of acid groups, we have

$$\frac{f_c^A(\mathbf{r})\rho_{H^+}(\mathbf{r})}{f_{uc}^A(\mathbf{r})\rho_s(\mathbf{r})} = {}^AK_a^o, \quad (23)$$

where ${}^AK_a{}^o$ is the thermodynamic equilibrium constant of the acid–base reaction,

$${}^AK_a^o = \exp(-\beta\Delta G^o) = \exp(-\beta(\mu_{H^+}^o + \mu_c^{o,A} - \mu_{uc}^{o,A})). \quad (24)$$

An analogous expression is obtained for the basic segments,

$$\frac{f_c^B(\mathbf{r})\rho_{OH^-}(\mathbf{r})}{f_{uc}^B(\mathbf{r})\rho_s(\mathbf{r})} = {}^BK_b^o, \quad (25)$$

where

$${}^BK_b^o = \exp(-\beta\Delta G^o) = \exp(-\beta(\mu_{OH^-}^o + \mu_c^{o,B} - \mu_{uc}^{o,B})). \quad (26)$$

In Eqs. (23) and (25), we assumed $v_s = v_{H^+} = v_{OH^-}$ (see Sec. II E below). Note that Eqs. (23) and (25) are the chemical equilibria equations corresponding to reactions (1) and (2), respectively. The thermodynamic equilibrium constants ${}^AK_a{}^o$ and ${}^BK_b{}^o$ can be related to the most commonly used equilibrium constants using molar concentrations, ${}^AK_a$ and ${}^BK_b$, by evaluating Eqs. (23) and (25) in the bulk solution (where $\rho_s v_s \approx 1$) and applying a multiplicative factor to change units. In this case, ${}^AK_a$ and ${}^BK_b$ are obtained by dividing ${}^AK_a{}^o$ and ${}^BK_b{}^o$ by a factor $c^o\ N_A{\cdot}v_s/(10^{24}\ nm^3/dm^3)$, where N_A is Avogadro's number and $c^o = 1M$ is the concentration of the standard reference state for ${}^AK_a$ and ${}^BK_b$. The constant for the dissociation of the base ${}^BK_b$ can then be converted into the constant for the dissociation of the conjugated acid (BH^+): ${}^BK_a = K_w/{}^BK_b$, where K_w is the equilibrium constant for the water self-dissociation reaction ($K_w = 10^{-14}$).

The equations for the interaction between the charged sites in the polyelectrolytes with salt ions are similar to Eqs. (23) and (25), although we opted to express them as association reactions instead of the dissociation reactions used in Eqs. (23) and (25) to describe acid–base reactions. For polymer A, the association of a negatively charged segment with a cation in solution is given by

$$\frac{f_{as\text{-}ion}^A(\mathbf{r})(\rho_s(\mathbf{r})v_s)^{(v_{Na^+}/v_s)}}{f_c^A(\mathbf{r})\rho_{Na^+}(\mathbf{r})v_s} = {}^AK_{as\text{-}ion}^o, \quad (27)$$

where ${}^AK^o{}_{as\text{-}ion}$ is the thermodynamic equilibrium constant of the association reaction (4),

$${}^AK_{as\text{-}ion}^o = \exp(\beta(\mu_{Na^+}^o + \mu_c^{o,A} - \mu_{as\text{-}ion}^{o,A})). \quad (28)$$

An analog expression holds for the association of a positively charged segment in polymer B and an anion in solution,

$$\frac{f_{as\text{-}ion}^B(\mathbf{r})(\rho_s(\mathbf{r})v_s)^{(v_{Cl^-}/v_s)}}{f_c^B(\mathbf{r})\rho_{Cl^-}(\mathbf{r})v_s} = {}^BK_{as\text{-}ion}^o, \quad (29)$$

where ${}^BK^o{}_{as\text{-}ion}$ is the thermodynamic equilibrium constant of the association reaction (5),

$${}^BK_{as\text{-}ion}^o = \exp(\beta(\mu_{Cl^-}^o + \mu_c^{o,B} - \mu_{as\text{-}ion}^{o,B})). \quad (30)$$

In this case, the thermodynamic equilibrium constants ${}^AK^0{}_{as\text{-}ion}$ and ${}^BK^0{}_{as\text{-}ion}$ can be converted to equilibrium constants in molar concentrations (${}^AK_{as\text{-}ion}$ and ${}^BK_{as\text{-}ion}$) by multiplying them by a factor $c^o{\cdot}N_A{\cdot}v_s/(10^{24}\ nm^3/dm^3)$.

The chemical equilibria equation for the ion-pairing reaction, reaction (3), is

$$\frac{f_{as}^A(\mathbf{r})}{f_c^A(\mathbf{r})f_c^B(\mathbf{r})\langle n_A(\mathbf{r})\rangle} = \frac{f_{as}^B(\mathbf{r})}{f_c^A(\mathbf{r})f_c^B(\mathbf{r})\langle n_B(\mathbf{r})\rangle} = K_{as}^o v_{AB}, \quad (31)$$

where $K^o{}_{as}$ is the thermodynamic equilibrium constant that regulates the polyion–polyion ion-pair formation, given by

$$K_{as}^o = \exp(-\beta(\mu_{as}^{o,A} + \mu_{as}^{o,B} - \mu_c^{o,B} - \mu_c^{o,A})). \quad (32)$$

Note that the volume of the complex, v_{AB}, can be absorbed into an effective equilibrium constant. The conversion of the constant $v_{AB}K^o{}_{as}$ to a constant in molar concentrations (K_{as}) requires the multiplication by a factor $c^o\ N_A/(10^{24}\ nm^3/dm^3)$.

Finally, the extremization of $\mathcal{L}$ with respect to the electrostatic potential, $\psi(\mathbf{r})$, gives the expression,

$$\epsilon\nabla^2\psi(\mathbf{r}) = -\langle\rho_q(\mathbf{r})\rangle \quad (33)$$

with the following boundary condition for the bulk:

$$\lim_{z\to\infty}\psi(\mathbf{r}) = 0, \quad (34)$$

and the boundary condition at the uncharged grafting surface:

$$\left.\frac{\partial\psi(\mathbf{r})}{\partial z}\right|_{z=0} = 0. \quad (35)$$

Note that Eq. (33) is analog to the Poisson equation with the difference that the charge density and the electrostatic potential are replaced by their ensemble-averaged quantities, $\langle\rho_q(\mathbf{r})\rangle$ and $\psi(\mathbf{r})$, respectively. While the Poisson equation is a fundamental equation of electrostatics and exactly describes the electrostatic potential of a given microstate, Eq. (33) is approximate. This mean-field electrostatic approach by itself can be inadequate to describe the behavior of mixtures of oppositely charged electrolytes, where strong correlations occur. For example, in a homogeneous solution of two oppositely charged polyelectrolytes, $\langle\rho_q\rangle = 0$ because of the requirement of phase electroneutrality and; therefore, the electrostatic potential

is constant and the electrostatic contribution to the free energy vanishes. The present theory allows for spatial inhomogeneities, but still two charges close enough (i.e., located at the same position within the resolution of our discretization scheme, see below) will cancel out. For these reasons, we introduced in the present theory the polyion–polyion ion pairs as a method to partially correct the underlying mean-field approach.

C. 1D-model approximation

The methodology described so far is the most general case for a system that presents inhomogeneities in the three spatial directions (x, y, and z). We will refer to this model hereafter as the 3D model. A commonly used approximation is to assume that the system is homogeneous in planes parallel to the grafting surface and, therefore, presents inhomogeneities only in the direction normal to it (the z coordinate).[50,54] We will refer to this approximation as the 1D model. The 1D model has the obvious advantage of being computationally less expensive than the 3D model, and, therefore, it allows us to perform a systematic exploration of the problem. By construction, the 1D model cannot describe the shape of microphase-separated aggregates, but it can provide the onset conditions for their formation, as discussed in Sec. III.

In order to formulate the 1D model from the 3D model, we simply assume that all functions that describe the structure of the system (ρ_i, ψ, f^i_c, f^i_{uc}, f^i_{as}, $f^i_{as\text{-}ion}$) depend only on the z coordinate. For example, Eq. (7) becomes

$$-S_{Trans}/(k_BA) = \sum_{i=H^+,OH^-,Na^+,Cl^-,s} \int \rho_i(z)[\ln(\rho_i(z)v_s) - 1]dz. \quad (36)$$

The case of $P_i(\alpha_i, j)$ requires special attention because in the 1D model the specific locations of the grafting points on the surface are lost and, therefore, the probability distribution function of chain conformations does not depend on the grafting position j anymore. The total number of grafting position in the system is equal to σ_iA, where σ_i is the grafting density (grafting points per unit area) of the chains of type i (i = A, B) and A is the area of the grafting surface. Therefore, Eq. (9) becomes

$$-S_{conf}/(k_BA) = \sigma_A \sum_{\alpha_A} P_A(\alpha_A)\ln(P_A(\alpha_A)) + \sigma_B \sum_{\alpha_B} P_B(\alpha_B)\ln(P_B(\alpha_B)), \quad (37)$$

and Eq. (12) is transformed to

$$\langle n_i(z)\rangle = \sigma_i \sum_{\alpha_i} P_i(\alpha_i) n_i(z;\alpha_i), \quad (38)$$

where $n_i(z, \alpha_i)dz$ is the number of segments that a chain of type i (i = A, B) has in the element volume between z and $z + dz$ when it is in conformation α_i. It should be noted that in this model, the grafting pattern is irrelevant because of the assumption of homogeneity in the plane parallel to the grafting surface.

Note that in Eqs. (36) and (37), the entropies are divided by the area of the system. The same is true for all terms in ω [Eq. (15)] and, therefore, the 1D model provides us free energy densities, ω/A.

D. Discretization and numerical solution of the theory

The equations of the theory are discretized in a cubic lattice of volume δ^3 (3D model) or in layers of thickness δ (1D model), where δ = 0.5 nm. The resulting set of equations is solved by replacing the equations resulting from the functional extrema of $\mathcal{L}$ [Eqs. (20)–(32)] into the packing constraints [Eq. (16)], the Poisson equation [Eq. (33)], and the ion-pairing stoichiometry constraint [Eq. (17)]. This procedure produces a set of $3M$ equations (where M is the number of cubic cells in the 3D model or planar layers in the 1D model) and $3M$ unknowns: the values of ϕ_s, ψ and $\langle n_A\rangle$ in each cell or layer of the system. This coupled system of non-linear equations is solved using numerical methods. The inputs of the theory are the molecular model, the properties of the solution (salt concentration and pH), and the grafted brush (surface coverage and chain length) and the set of randomly generated polymer conformations. As an output, we obtain structural and thermodynamic information on the system.

E. Molecular model

We generated a set of 10^6 random polymer conformations using the rotational isomeric state (RIS) model[55] with a segment length of 0.8 nm. The bulk pK_a values (acid–base equilibrium constants) for the acid and base groups were set to 5 and 9, respectively. The dielectric constant ϵ was set to that of water 78.5ϵ_0 everywhere in the system, which is a good approximation for polyelectrolyte brushes.[50] The volumes of salt ions (ν_{Na+} and ν_{Cl-}), solvent molecules (ν_s), and polymer segments (ν_p) were set to 0.08 nm^3, 0.03 nm^3 and 0.06 nm^3, respectively.

III. RESULTS

A. Structure of the mixed polyelectrolyte brush

In Fig. 2, we analyze the structure of the mixed polyelectrolyte brush determined with the 1D model. The polyacid and polybase are symmetric in our system because we chose to use the same chain length (N) and surface coverage (σ) for both polymers. We chose their pK_a values (acid–base equilibrium constants) to be $^{A}pK_a$ = 5 and $^{B}pK_a$ = 9, respectively, and, therefore, the system is fully symmetric for pH = 7, where both polymers bear the same charge. Figures 2(a) and 2(b) show the volume fraction of the polyacid (polyA) and the polybase (polyB) as a function of the distance from the grafting surface for values of pK_{as} = 5 and −1.6 and pH = 7, respectively. The value of pK_{as} determines the polyion–polyion ion-pairing constant K_{as}, pK_{as} = −log$_{10}$(K_{as}); therefore, a more positive pK_{as} indicates weaker ion-pairing. In Fig. 2, as well as in other cases discussed in this section, we assume that the association between the polyelectrolyte and salt ions is very weak, and, therefore, ion–polyion association is neglected (the effect of the ion–polyion ion pairs will be discussed in Sec. III B). The insets of Figs. 2(a) and 2(b) show that the fraction of associated segments as a function of the distance to the grafting surface. For pK_{as} = 5, the formation of ion pairs is weak, the degree of association of both polyelectrolytes is close to zero [inset in Fig. 2(a)], and the predictions of our theory are in line to previous work that did not explicitly considered ion-pairing interactions.[32,33] At pH = 7 and pK_{as} = 5, the

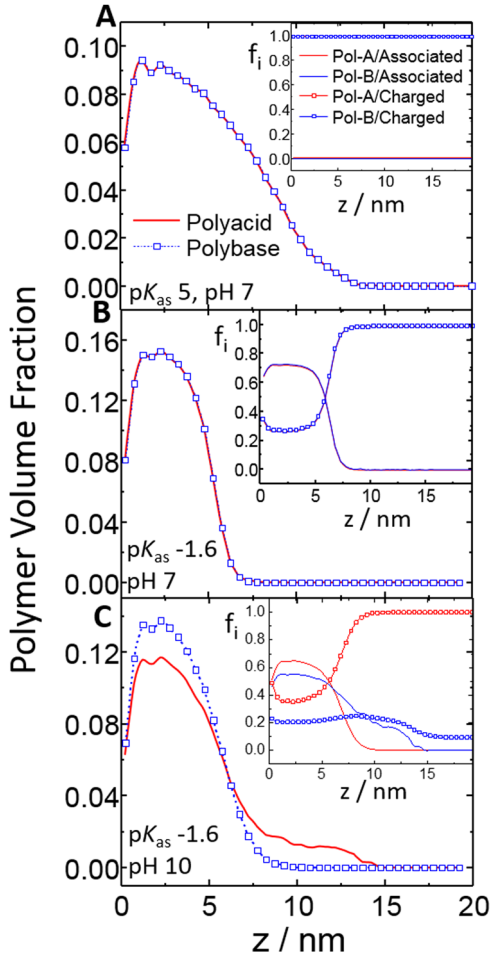

FIG. 2. The volume fraction of the polyacid and the polybase as a function of the distance to the surface calculated with the 1D model for pH = 7 [panels (a) and (b)] and 10 [panel (c)] and pK_{as} = 5 [panel (a)] and −1.6 [panels (b) and (c)], where $pK_{as} = -\log_{10}(K_{as})$. K_{as} is the equilibrium constant of the polyion–polyion association reaction (larger values of pK_{as} indicate weaker polyion–polyion ion pairs). Inset: fraction of associated segments in the polyacid and the polybase, f_{as}^{i} (i = A, B), as a function of the distance from the surface. Note that in panels (a) and (b), $|\text{pH} - pK_a| = 2$ for both the polyacid and the polybase, and, therefore, the system is symmetric and the volume fraction of the polymers and fraction of associated segments of the polyacid and polybase are the same. Calculation conditions: pK_a polyacid = 5, pK_a polybase = 9, N = 30, salt concentration 0.1M, surface coverage $\sigma_A = \sigma_B$ = 0.4 chain nm^{-2}, and no ion–polyion association.

brush extends up to ~13 nm from the surface. Note that a pure polyacid or pure polybase brush under the same conditions is more stretched than the mixed brush (up to ~14 nm, see Fig. S1 in the supplementary material). Pure polyacid or polybase brushes swell because of the osmotic pressure of the mobile counterions required to balance the charges of the polyelectrolyte.[56] On the other hand, in the symmetric mixed brush, the compensation of polyelectrolyte charges results in a smaller degree of swelling than in the single-component layer, even when ion-pairing interactions are absent ($K_{as} \ll 1$).

The formation of ion-pairs, which is not captured by standard electrostatic mean-field interactions, is considered in the present theory as a chemical association equilibrium; see Eq. (3). Figure 2(b) shows results for pH = 7 and $pK_{as} = -1.6$. Under these conditions, ~70% of the polyelectrolyte charges participate in polyion–polyion ion pairs (see the inset). The density profile in Fig. 2(b) shows that the brush is considerably more collapsed than the case with pK_{as} = 5 in Fig. 2(a). Figure 2(c) shows the volume-fraction profiles for $pK_{as} = -1.6$ and pH = 10. Under these conditions, the polyacid ($p^{A}K_a$ = 5) is fully charged while the polybase ($p^{B}K_a$ = 9) is not. The polyacid, therefore, is more stretched than the polybase. In the region $0 < z < 6$ nm, the fraction of the associated acid segments is higher than that of the associated base segments [$f_{as}^{B} < f_{as}^{A}$, see the inset in Fig. 2(c)] and the opposite behavior is observed for $z > 6$ nm. This result is a consequence of the stoichiometry constraint, Eq. (17), which enforces that the total number of associated acid and basic segments to be the same locally. In other words, when the total local density of a given type of segment increases (and the density of segments of the other type remains fixed), the fraction of those segments in the associated state should decrease.

Let us analyze in detail the population of each possible chemical state of the polyelectrolyte segments: (i) charged and unassociated (pol-A^- for the polyacid, pol-BH^+ for the polybase), (ii) uncharged (pol-AH for the polyacid, pol-B for the polybase), (iii) associated in a polyion–polyion ion pair ([pol-$A^-\cdots$pol-BH^+] complex), and (iv) associated in an ion–polyion ion pair (pol-A^-Na^+ and pol-BH^+Cl^-; corresponds to a charged polyelectrolyte group with a condensed counterion). The population of the latter state is negligible for the results shown in this section because we used very small ion–polyion association constants ($^{A}K_{\text{as-ion}}$, $^{B}K_{\text{as-ion}} \ll 1$, i.e., we neglected polyion–ion association in these calculations). In Fig. 3, we analyze how the populations of the other three chemical states (charged, uncharged, and associated) are controlled by the pH and the polyelectrolyte–polyelectrolyte ion-pairing association constant, K_{as}. In Fig. 3, the chemical state of the polyelectrolyte segments is summarized in terms of their average fractions, defined as

$$\langle f_i^p \rangle = \frac{\int f_i^p(z)\langle n_p(z)\rangle dz}{\int \langle n_p(z)\rangle dz}, \tag{39}$$

where i = c, uc, and as for charged, uncharged, and associated segments, respectively, and p = A, B for the polyacid and the polybase, respectively. Note that in Fig. 3, $\langle f_{as}^{A}\rangle = \langle f_{as}^{B}\rangle$ under all conditions. This result is a consequence of the stoichiometry constraint: even when the fractions of associated segments $f_{as}^{A}(z)$ and $f_{as}^{B}(z)$ can differ locally [e.g., results shown in the inset of Fig. 2(c)], the stoichiometry condition given by Eq. (17) results always in $\langle f_{as}^{A}\rangle = \langle f_{as}^{B}\rangle$ [this result can be easily demonstrated by replacing Eq. (17) into Eq. (39)].

For pK_{as} = 5 ($K_{as} = 10^{-5}$), the ion-pairing interaction is very weak and, therefore, the fraction of associated segments is close to zero for all pHs. The fraction of charged species follows the typical acid–base speciation curve. On the other hand, under strong association conditions, $pK_{as} = -2$, the ion-pairing interaction produces a significant fraction of associated segments. The fraction of associated segments has a maximum at pH 7, where both the

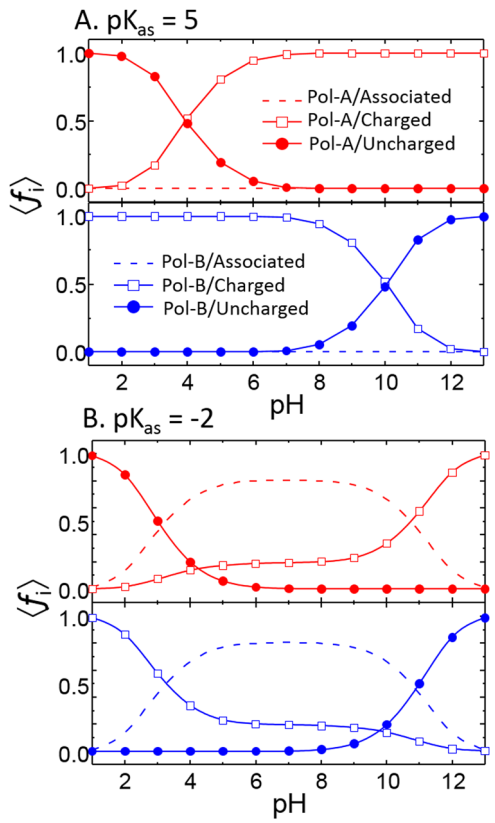

FIG. 3. Average fractions of charged, uncharged, and associated segments for the polyacid and the polybase as a function of pH for pK_{as} = 5 [panel (a), weak polyion–polyion ion pairing] and −2 [panel (b), strong polyion–polyion ion pairing].

polyacid and the polybase are highly charged. As the pH is increased from this value, the acid–base equilibrium of the basic segments is shifted toward the uncharged species and the fraction of charged pol-BH^+ species decreases. This decrease shifts the ion-pairing association equilibria [Eq. (3)] toward the unassociated state. A similar argument holds for the effect of decreasing pH from the optimum value of pH = 7. Note, however, that the associated state can dominate the population even under conditions where the fraction of charged free segments is much smaller than that of the neutral free state (e.g., pH 4 for the polyacid and pH 10 for the polybase).

B. Microphase separation due to ion-pairing interactions

So far, we have shown that the 1D model predicts the collapse of the mixed brush upon increasing the strength of ion pairing. The question that arises is whether this interaction can lead to microphase separation of the mixed brush, even when both polyelectrolytes are in a good solvent (i.e., there are no effective van der Waals attractions between segments). It is well known that a mixture of polyanions and polycations in solution can phase separate forming a polymer rich phase (polyelectrolyte coacervate) and a polymer-poor solution.[1,2,31,34,36] This type of macroscopic phase separation clearly cannot occur in a mixed brush due to the constraint introduced by the grafting points; however, the system can microphase separate, forming micro- or nanometer-sized domains on the surface. Carignano and Szleifer[57] have demonstrated that it is possible to estimate the onset of microphase separation in a polymer brush using a 1D model, as we explain below.

Let us consider the thermodynamics of the system in Fig. 1 in terms of the following thermodynamic variables: n_A (number of grafted polyacid chains), n_B (number of grafted polybase chains), T (temperature), A (area), and μ_i (chemical potential of free species, i = s, H^+, OH^-, Na^+ and Cl^-). Note that this description of the system is just approximate for a polymer brush, where the number of polyelectrolyte chains is not a proper thermodynamic variable because it cannot be controlled by changing an intrinsic thermodynamically conjugated variable (i.e., its chemical potential). In other words, the following derivation is strictly valid for a system with laterally mobile chains. However, in a previous study,[47] we have shown that this argument can predict the onset of microphase separation of polymer brushes from 1D-model calculations in very good agreement with fully 3D calculations.

The thermodynamic potential for the system described in the previous paragraph is the semi-grand canonical free energy, ω [given by Eq. (15)]. The differential of ω as a function of those of its natural thermodynamic variables is

$$d\omega = -\Pi dA + \mu_A dn_A + \mu_B dn_B + SdT + \sum_{i=s,H^+,OH^-,Na^+,Cl^-} n_i d\mu_i, \quad (40)$$

where Π is the lateral pressure. Euler integration results in

$$\omega[A, n_A, n_B, T, \{\mu_i\}] = -\Pi A + \mu_A n_A + \mu_B n_B. \quad (41)$$

In order to be thermodynamically stable with respect to the formation of lateral inhomogeneities, a laterally homogeneous system should fulfill the condition,

$$\left.\frac{\partial \Pi}{\partial A}\right)_{n_A,n_B,T,\{\mu_i\}} = -\frac{\sigma}{A}\left.\frac{\partial \Pi}{\partial \sigma}\right)_{x_B,T,\{\mu_i\}} < 0, \quad (42)$$

where in the second equality, we transformed the derivative with respect to the area A (extensive variable) to a derivative with respect to the intensive variable,[58] $\sigma = (n_A + n_B)/A = \sigma_A + \sigma_B$ and x_B is the molar fraction of the polybase on the surface, $x_B = n_B/(n_A + n_B) = {}_B/\sigma$.

The lateral pressure results from[57]

$$\Pi = -\left.\frac{\partial \omega}{\partial A}\right)_{n_A,n_B,T,\{\mu_i\}} = -A\left.\frac{\partial \omega/A}{\partial A}\right)_{n_A,n_B,T,\{\mu_i\}} - \omega/A$$
$$= \sigma\left.\frac{\partial \omega/A}{\partial \sigma}\right)_{x_B,T,\{\mu_i\}} - \omega/A. \quad (43)$$

Note that the partial derivatives in Eqs. (42) and (43) are done at constant x_B (i.e., constant surface composition). The calculation of Π requires the free energy density, ω/A, which is straightforwardly obtained from the 1D-model molecular theory calculation, as a function of the total surface coverage (σ) for a fixed brush composition (x_B). According to Eq. (42), a system of laterally mobile chains will be stable with respect to lateral phase separation when $\Pi(\sigma)$ is a monotonically increasing function. It can be shown that in the case

of a single-component system, Eqs. (42) and (43) result in a condition over the slope of the chemical potential of the polymer (see the supplementary material). In other words, the stability criterion based on $\Pi(\sigma)$ is more general than that based on $\mu(\sigma)$, and these two criteria become equivalent only when there is only one type of polymer chain in the system. In previous studies,[46,47,52] the condition over the chemical potential has been proved to correctly capture the onset of microphase separation of the grafted polymer and polyelectrolyte brushes under poor-solvent conditions. Therefore, the condition of $\Pi(\sigma)$ being a monotonically increasing function will be used in the rest of this work as an approximate criterion for the thermodynamic stability of the homogeneous polyanion/polycation brush. In Sec. III C, this criterion is validated by comparing the predictions of Eq. (43) for the mixed polyanion/polycation brush against the predictions of the 3D model.

Figure 4(a) shows the theoretical predictions for the lateral pressure, Π, of the mixed brush at pH = 7 as a function of the total surface coverage, σ, for different values of the polyion–polyion ion-pairing equilibrium constant. Interestingly, in the system where ion-pairing interactions are negligible ($pK_{as} = 5$, $K_{as} = 10^{-5}$), Π monotonically increases with σ. This result is important because it indicates that a mean-field treatment of electrostatics without including ion-pairing interactions cannot capture the formation of lateral aggregates in mixed polyacid/polybase brushes. On the other hand, for $pK_{as} < -0.4$ ($K_{as} > 2.51$), the Π vs σ curve exhibits a minimum at a critical value, σ_{crit}. For $\sigma < \sigma_{crit}$, the condition given by Eq. (42) suggests that the laterally homogeneous film is unstable and, therefore, microphase separation is expected. In summary, microphase separation is predicted for mixed polyanion/polycation brushes only when the possibility of ion-pairing interactions is explicitly accounted for. The formation of lateral inhomogeneities predicted by our theory may explain the observation of ripple-like morphologies in the AFM experiments of Ref. 13. Interestingly, experiments and theory have shown that ion pairing is responsible for the formation of lateral aggregates in a related system: single-component polyelectrolyte brushes immersed in a solution of multivalent ions.[59] In that case, however, self-assembly into aggregates is triggered by the formation of ion pairs between the polyelectrolyte and the multivalent ion in solution rather than by complexation between two oppositely charged polyelectrolytes grafted on the same surface.

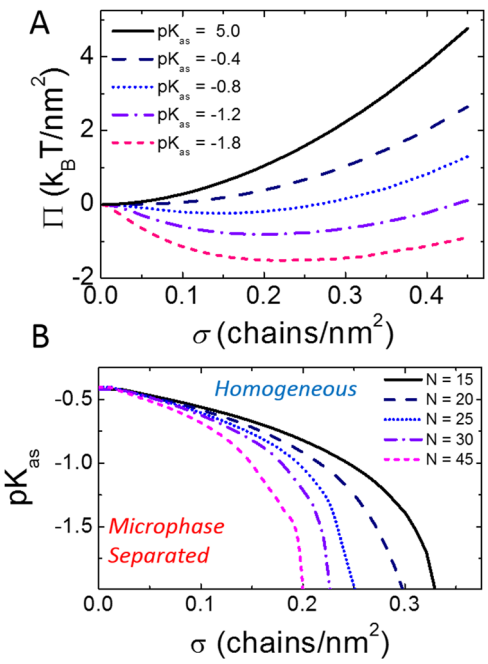

FIG. 4. (a) Lateral pressure of the grafted polyelectrolyte molecules as a function of the total surface coverage, σ ($\sigma = \sigma_A + \sigma_B$) for a constant surface composition ($\sigma_A = \sigma_B$) and different values of the polyion–polyion ion-pair association constant, pK_{as}. (b) Stability diagram for the mixed polyelectrolyte brush derived from condition in Eq. (42), showing the stability of the homogeneous brush and the inhomogeneous, microphase-separated brush as a function of σ and pK_{as} for different values of the polyelectrolyte chain length, N (the polyacid and the polybase have the same chain length). Calculation conditions: salt concentration 0.1M, $N = 30$ [panel (a) only], pH = 7, $p^AK_a = 5$, $p^BK_a = 9$ and no ion–polyion association.

When the total polyelectrolyte surface coverage is smaller than the critical value (minimum of the Π vs σ curve), the system is predicted to form nanometric aggregates and become laterally inhomogeneous. Figure 4(b) shows the curves of stability of the homogeneous brush in the pK_{as} vs σ_{crit} plane for different chain lengths, N (both the polyanion and polycation chains have the same length). Note that below these curves, the homogeneous brush is predicted to be thermodynamically unstable, and, thus, it should microphase separate. In this regard, these curves indicate the "spinodal" stability of the system, although they are not real spinodal curves from the thermodynamic point of view because there are not two well-defined phases in equilibrium and because Eq. (42) is not a strict criterion of stability for grafted chains, as we discussed above. We observe that increasing N leads to a decrease in the surface coverage required for microphase separation and, therefore, to an increase in the stability of the homogeneous-brush morphology. This same trend was observed for the microphase separation of polymer brushes under poor-solvent conditions,[46] and it can be explained by considering that long chains can easily collapse to form a homogeneous layer, while short chains have limited extension, and, therefore, they tend to form aggregates upon collapsing. Interestingly, one AFM study of mixed polybase/polyacid (4PVP/PAA) brushes has shown a ripple morphology (attributed to a laterally segregated structure),[13] while in another study, a flat non-segregated surface was observed.[14] Based on the results of Fig. 4(b), we hypothesize that the different morphologies observed in these two studies may result from using different degrees of polymerization and/or surface coverages, so the conditions of the first study may be in the microphase separation regime, while those in the second one may be not.

In Fig. 5, we analyze the effect of pH on the stability of the homogeneous brush. It is interesting to mention that under some conditions [e.g., pH 4 and $N = 30$, see Fig. 5(a)], the Π vs σ plot differs from the example shown for pH 7 in Fig. 4(a) in the fact that the curve has two critical values for which $d\Pi/d\sigma = 0$ (i.e., it forms a van der Waals loop) instead of one. In those cases, microphase separation is predicted to occur between the two values of σ_{crit}. The effect of pH on the morphology diagram is summarized in Fig. 5(b). As expected from the acid–base constants of each segment type ($p^AK_a = 5$ and $p^BK_a = 9$), there is a symmetry in the morphology diagram

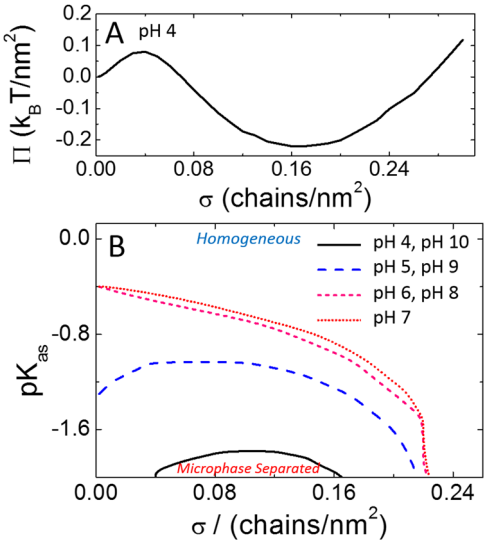

FIG. 5. (a) Lateral pressure of the grafted polyelectrolyte molecules as a function of the total surface coverage, σ for pH = 4. (b) Stability diagram for the mixed polyelectrolyte brush as a function of σ (for $\sigma_A = \sigma_B$) and pK_{as} for different values of pH. Calculation conditions: $pK_{as} = -2$ [panel (a) only], salt concentration 0.1M, $N = 30$, $p^AK_a = 5$, $p^BK_a = 9$, and no ion–polyion association.

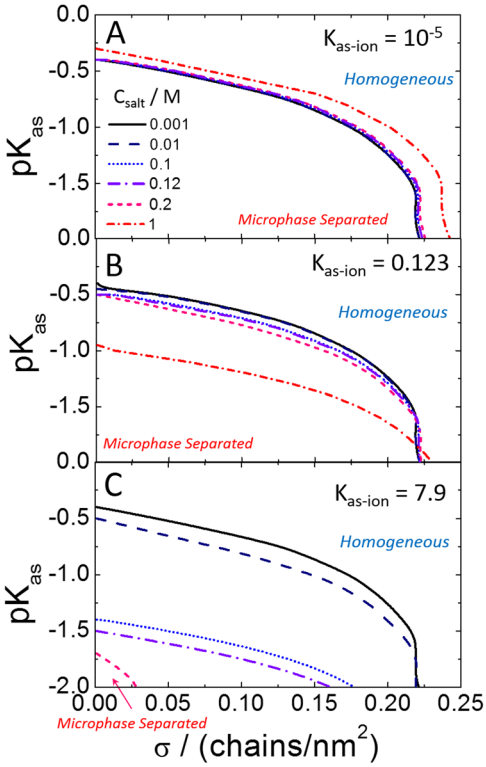

FIG. 6. Effect of salt concentration on the stability diagrams of the mixed polyacid/polybase brush as a function of σ (for $\sigma_A = \sigma_B$) and pK_{as} for different values of the ion–polyion association constant: ${}^AK_{as\text{-}ion} = {}^BK_{as\text{-}ion} = 10^{-5}$ [(a), ion–polyion association does not occur under this condition], ${}^AK_{as\text{-}ion} = {}^BK_{as\text{-}ion} = 0.123$ (b), and ${}^AK_{as\text{-}ion} = {}^BK_{as\text{-}ion} = 7.9$ (c). In (c), the curve for $C_{salt} = 1$M is not shown because the homogeneous brush is stable in the whole pK_{as}–σ region under study. Calculation conditions: pH = 7, $N_A = N_B = 30$, $p^AK_a = 5$, and $p^BK_a = 9$.

with respect to pH = 7. The predictions show that the microphase separation is most effective at pH = 7, because, as we have shown above, at this pH the fraction of associated segments is maximized. The fact the homogeneous brush is more stable under asymmetric conditions (pH 4 and 10) than under symmetric ones (pH 7) does not imply that polyion–polyion pairing has a negligible effect on the structure of the brush in the former case: in Fig. S3 in the supplementary material, we show that pK_{as} affects the morphology of the brush for pH 4, even when the homogeneous brush is the stable morphology.

Figure 5(b) shows that at low pH, the homogeneous brush becomes stable at low surface coverages (a reentrant behavior). A similar behavior has been previously predicted for single-component weak polyelectrolyte brushes in a poor solvent.[46] We stress that our model does not consider short-range hydrophobic interactions and, therefore, microphase separation is only attributable to the formation of polyion–polyion ion pairs. However, the origin of the reentrant behavior observed for pH < 5 in the present system seems to be the same as that described for single-component brushes in poor solvent. At pH < 5, the charge of the polycation is in excess to that of the polyanion. Under these conditions, the electrostatic repulsions among polycations reduce their charge via the charge-regulation mechanism.[46,47,60] Decreasing the surface coverage results in a decrease in polycation–polycation repulsions and, therefore, in an increase in the fraction of charged segments. This increase in the fraction of ionized polycation segments increases the solubility of the layer, stabilizing the homogeneous brush and giving rise to the reentrant behavior.

In Fig. 6, we analyze the role of salt concentration (C_{salt}) on the morphology of the brush. For very small values of the ion–polyion association constant, $K_{as\text{-}ion} = 10^{-5}$ (the same value was used for the polyacid and the polybase), ion–polyion ion pairs are not formed (i.e., same situation as in Figs. 2–5). Figure 6(a) shows that in this case, the formation of lateral aggregates is insensitive to salt concentration up to a 0.1M concentration, and for $C_{salt} = 1$M, the homogeneous phase is slightly de-stabilized. This result does not agree with experimental observations of the effect of salt on polyelectrolyte complexes,[1,3,24,29–31] which show that salt addition leads to the dissolution of polyelectrolyte complexes in solution and polyelectrolyte multilayers on surfaces. Destabilization of polyelectrolyte complexes by salt is, in general, ascribed to the disruption of polyion–polyion ion pairs by the formation of ion–polyion ion pairs,

$$Na^+ + Cl^- + [\text{Pol–A}^-\text{Pol–BH}^+] \rightleftharpoons \text{Pol–A}^-Na^+ + \text{Pol–BH}^+Cl^-. \quad (44)$$

Therefore, increasing the salt concentration is expected to stabilize the homogeneous phase instead of destabilizing it [as predicted by our theory for $K_{as\text{-}ion} = 10^{-5}$ in Fig. 6(a)]. The correct trend can be recovered in our theory by increasing the value of the ion–polyion association constant, $K_{as\text{-}ion}$. For example, Figs. 6(b) and 6(c) shows the morphology diagrams for $K_{as\text{-}ion} = 0.123$ [value

for the association constant of carboxylates and Na^+ determined from molecular dynamics (MD) simulations in Ref. 45] and 7.9, respectively. In these diagrams, an increase in the salt concentration leads to the expected stabilization of the homogeneous phase. We would like to mention that the choice of $K_{as\text{-}ion}$ does not have a qualitative effect on the phase-diagrams where the salt concentration is fixed (results in Figs. 2–5), although it changes the results quantitatively (i.e., increasing $K_{as\text{-}ion}$ leads to an increase in the value of K_{as} required for microphase separation). In summary, the results in Fig. 6 shows that the effect of ionic strength is only correctly captured by our ion-pairing formalism when the formation of ion pairs between salt ions and polyion charges is explicitly considered.

At this point, it is important to discuss two aspects of our theory. First, we have omitted the possibility of ion-pair formation between salt ions in solution (e.g., $Na^+ + Cl^- \rightleftharpoons [NaCl]$). The association constant for this process has been estimated to be $0.6M^{-1}$.[61] The fraction of associated ions will be ~5% in a 0.1M solution, but it will increase to ~30% in a 1M solution; therefore, this effect will be relevant only in very saline solutions. In that case, its effect will be to decrease the real concentration of free salt ions, thus displacing the chemical equilibrium in Eq. (44) to the left. For simplicity, we omitted the association between free ions in the present work, but its inclusion may be eventually necessary to quantitatively reproduce experimental measurements. This observation brings us to a second important point: the choice of the values of the ion-pair association constants, K_{as} (polyion–polyion association) and $K_{as\text{-}ion}$ (ion–polyion association). In this work, we decided to scan the values of these constants to study their qualitative effect on a model system. In order to make quantitative predictions on a specific system, these constants should either be obtained by fitting the experimental data[31] or estimated by other theoretical methods, such as molecular dynamics simulations.[45,61] Salehi and Larson[31] reported values for the polyion–polyion and ion–polyion association constants obtained by fitting the phase diagram of polyelectrolyte coacervates. We note that the theory in Ref. 31 was developed for polyelectrolytes in solution and contains contributions that were not included in our theory (such as hydrophobic interactions and Debye–Hückel ionic activities). Therefore, the order of magnitude of the values in that work can be compared with the values scanned here; however, the exact values cannot be straightforwardly used as an input for our theory. For the system poly(acrylic acid)/poly(diallyldimethylammonium), Salehi and Larson reported $pK_{as} = -2.9$ (data in Table 2 of Ref. 31, note that the reported K_{ip}^{∞} was divided by 55.56 to convert it to the molar reference state) and $K_{as\text{-}ion} = 77–194$ ($pK_{as\text{-}ion} = -1.89–2.29$). These values are around one pK unit more negative than the values explored in Fig. 5(c).

C. Comparison between 1D and 3D models

To confirm the validity of using the 1D model together with Eq. (42) to estimate the onset of microphase separation, we performed calculations with the 3D model, which allows inhomogeneities in the three spatial directions. The positions of the grafting points are irrelevant in the 1D model because homogeneity in the planes parallel to the substrate is assumed (i.e., the 1D model cannot distinguish different grafting patterns). However, the explicit grafting positions should be defined in the 3D model. For all calculations in this section, we produced a square arrangement of grafting points. We grafted one polycation and one polyanion chain at each grafting position (experimentally, such arrangement can be obtained using Y-shaped initiators[62,63]). Both polyions have the same chain length ($N = 30$) and we used pH = 7, so the properties of the polyacid and polybase are symmetric. This situation corresponds to a very symmetric system, which greatly facilitated the convergence of the 3D-model calculations. In general, we failed to converge less symmetric cases involving other pHs, unequal chain lengths, or other grafting point arrangements. We believe that this failure is of numerical nature rather than an intrinsic problem with our theory. Because we imposed symmetric properties for the polyacid and polybase chains and used a Y-grafting arrangement, the densities of the polycation and polyanion segments are the same locally. This latter condition allowed us to simplify the equations of the theory and converge the numerical problem (this condition is also true because we also used the same set of conformations for both types of polyelectrolytes).

Figures 7(a) and 7(b) show the morphology of the system predicted by the 3D model for a microphase separated system (polyion–polyion association constant $pK_{as} = -2$) and the homogeneous case ($pK_{as} = -1$), respectively. In both cases, $\sigma = 0.125$ nm^{-2}. The microphase separated case shows aggregates that are similar in shape

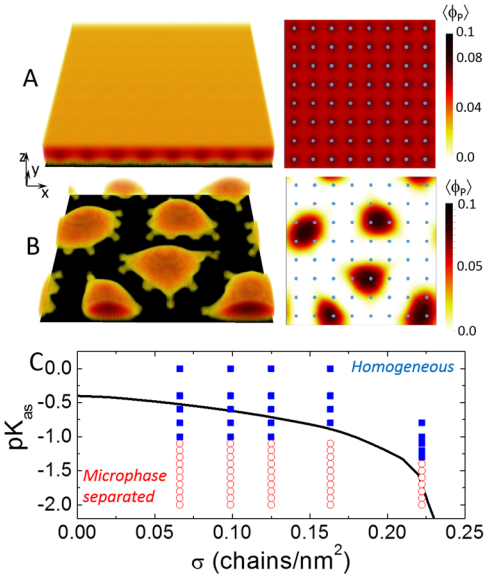

FIG. 7. [(a) and (b)] Homogeneous brush [panel (a)] and microphase-separated aggregates [panel (b)] obtained using the 3D model for a mixed polyelectrolyte brush. The right panels show color maps of the total polymer volume fraction (sum of the volume fractions of A-type and B-type segments) in a cut along a plane normal to the substrate. Blue dots indicate the position of the grafting points (each grafting point has one polyanion and one polycation chain of the same length, see text). The left panels show a perspective representation of the morphologies. (c) Morphology diagram comparing the predictions of the 1D model (black line) and the 3D model (blue solid squares for homogeneous brush and red empty squares for the aggregates) as a function of the total grafting density, σ, and the polyion–polyion association constant, pK_{as}.

and size to those obtained for single-polymer brushes under poor solvent conditions in previous works.[47,52] This result suggests that the size of the aggregates is likely controlled by the surface density and chain length (which are similar in the present work and previous works for brushes in poor solvent) rather than by the mechanism of aggregation. Note that in the present case, each aggregate contains both polycation and polyanion chains.

Figure 7(c) shows a comparison of the morphology diagrams predicted in the pK_{as} vs σ plane by the 1D model (solid black line) and the 3D model (symbols). We should mention that, under some conditions, we were able to converge both the homogeneous and aggregated morphologies, but in those cases, we always observed that the microphase-separated system had the smallest free energy (see supplementary material). Generally speaking, the stability curve predicted by the 1D model is in good agreement with the predictions of the 3D model, although it tends to overestimate the stability of the microphase-separated region for low surface coverages ($\sigma < 0.2$ nm^{-2}) and to underestimate it for high ones, $\sigma > 0.2$ nm^{-2}.

IV. CONCLUSIONS

We developed a molecular theory to study mixtures of polyacids and polybases at interfaces and used it to model a mixed polyelectrolyte brush. In order to overcome the well-known limitation of the mean-field theories to deal with polyelectrolyte complexation, we explicitly included in our theory the formation of ion pairs between the charges of the polyions. Notably, the inclusion of polyion–polyion ion pairs in the theory enables the formation of lateral aggregates (microphase separation). These aggregates may explain the ripples observed by the recent AFM experiments.[13] We have also shown the importance of considering the formation of ion pairs between polyion charges and salt ions in solution to properly capture the rupture of polyion–polyion ion bonds with an increase in ionic strength.

We analyzed the effect of pH, salt concentration, chain length, and surface coverage in the microphase separation of mixed brushes. The formation of lateral aggregates is favored when both polyions are highly charged, which in the case of the present study occurs at pH 7. Increasing the density of the polyelectrolyte segments, either by increasing the chain length or the surface coverage, results in most cases in a stabilization of the homogeneous brush. However, at low pH (pH < 5) and high pH (pH > 9), the mixed brush exhibits reentrant stability: the homogeneous brush stabilizes at low values of surface coverage.

In summary, we have demonstrated the usefulness of including the formation of polyion–polyion ion pairs via an association reaction formalism within a molecular theory. We believe that this simple strategy can be useful in the future to address other systems of interest where polycation–polyanion interactions are dominant, such as polyelectrolyte coacervates in solution or multilayer films obtained by layer-by-layer deposition of polyelectrolytes.

SUPPLEMENTARY MATERIAL

See the supplementary material for polymer volume–fraction profiles of single-component polyelectrolyte brushes, thermodynamic criteria for microphase separation of a single-component brush in terms of its chemical potential, a comparison of the free energy of the microphase-separated and the homogeneous brush in 3D model calculations, volume fraction profiles for asymmetric conditions (pH 4) as a function of pK_{as}, and the derivation of the chemical-equilibrium contribution to the free energy.

ACKNOWLEDGMENTS

M.T. is a fellow of CONICET. M.T. acknowledges financial support from the Agencia Nacional de Promoción Científica y Tecnológica (ANPCyT) (Grant Nos. PICT-0154-2016 and PICT 4649-2018) and the University of Buenos Aires (Grant No. UBACYT 20020170200215BA).

DATA AVAILABILITY

The unprocessed data from the calculations and the computer code used to run them are available from the corresponding author upon reasonable request.

REFERENCES

[1] R. Chollakup, W. Smitthipong, C. D. Eisenbach, and M. Tirrell, Macromolecules **43**, 2518 (2010).
[2] Q. Wang and J. B. Schlenoff, Macromolecules **47**, 3108 (2014).
[3] C. E. Sing and S. L. Perry, Soft Matter **16**, 2885 (2020).
[4] G. Decher and J. B. Schlenoff, *Multilayer Thin Films: Sequential Assembly of Nanocomposite Materials* (John Wiley & Sons, 2006).
[5] Z. Ou and M. Muthukumar, J. Chem. Phys. **124**, 154902 (2006).
[6] J. J. Cerdà, B. Qiao, and C. Holm, Soft Matter **5**, 4412 (2009).
[7] J. Fu and J. B. Schlenoff, J. Am. Chem. Soc. **138**, 980 (2016).
[8] C. F. Narambuena, D. M. Beltramo, and E. P. M. Leiva, Macromolecules **41**, 8267 (2008).
[9] N. Houbenov, S. Minko, and M. Stamm, Macromolecules **36**, 5897 (2003).
[10] L. Ionov, N. Houbenov, A. Sidorenko, M. Stamm, I. Luzinov, and S. Minko, Langmuir **20**, 9916 (2004).
[11] Y. Mikhaylova, L. Ionov, J. Rappich, M. Gensch, N. Esser, S. Minko, K.-J. Eichhorn, M. Stamm, and K. Hinrichs, Anal. Chem. **79**, 7676 (2007).
[12] K. Hinrichs, D. Aulich, L. Ionov, N. Esser, K.-J. Eichhorn, M. Motornov, M. Stamm, and S. Minko, Langmuir **25**, 10987 (2009).
[13] A. Drechsler, M. M. Elmahdy, P. Uhlmann, and M. Stamm, Langmuir **34**, 4739 (2018).
[14] M. Motornov, T. Kin Tam, M. Pita, I. Tokarev, E. Katz, and S. Minko, Nanotechnology **20**, 434006 (2009).
[15] D. R. M. Williams, J. Phys. II **3**, 1313 (1993).
[16] O. Peleg, M. Tagliazucchi, M. Kröger, Y. Rabin, and I. Szleifer, ACS Nano **5**, 4737 (2011).
[17] S. L. Turgeon, C. Schmitt, and C. Sanchez, Curr. Opin. Colloid Interface Sci. **12**, 166 (2007).
[18] C. Schmitt and S. L. Turgeon, Adv. Colloid Interface Sci. **167**, 63 (2011).
[19] C. P. Brangwynne, P. Tompa, and R. V. Pappu, Nat. Phys. **11**, 899 (2015).
[20] Y. Shin and C. P. Brangwynne, Science **357**, eaaf4382 (2017).
[21] T. Lu and E. Spruijt, J. Am. Chem. Soc. **142**, 2905 (2020).
[22] Q. Zhao, D. W. Lee, B. K. Ahn, S. Seo, Y. Kaufman, J. N. Israelachvili, and J. H. Waite, Nat. Mater. **15**, 407 (2016).
[23] G. Decher, Science **277**, 1232 (1997).
[24] E. Spruijt, M. A. Cohen Stuart, and J. van der Gucht, Macromolecules **43**, 1543 (2010).
[25] M. Kobayashi, M. Terada, and A. Takahara, Soft Matter **7**, 5717 (2011).
[26] M. Raftari, Z. J. Zhang, S. R. Carter, G. J. Leggett, and M. Geoghegan, Macromolecules **48**, 6272 (2015).

[27]P. Uhlmann, N. Houbenov, N. Brenner, K. Grundke, S. Burkert, and M. Stamm, Langmuir **23**, 57 (2007).
[28]O. Azzaroni and I. Szleifer, *Polymer and Biopolymer Brushes: For Materials Science and Biotechnology* (John Wiley & Sons, 2018).
[29]J. Heuvingh, M. Zappa, and A. Fery, Langmuir **21**, 3165 (2005).
[30]S. T. Dubas and J. B. Schlenoff, Langmuir **17**, 7725 (2001).
[31]A. Salehi and R. G. Larson, Macromolecules **49**, 9706 (2016).
[32]N. P. Shusharina and P. Linse, Eur. Phys. J. E **6**, 147 (2001).
[33]X.-j. Zhao and G.-l. Zhang, Chin. J. Polym. Sci. **32**, 568 (2014).
[34]C. E. Sing, Adv. Colloid Interface Sci. **239**, 2 (2017).
[35]M. Castelnovo and J.-F. Joanny, Eur. Phys. J. E **6**, 377 (2001).
[36]A. Kudlay, A. V. Ermoshkin, and M. Olvera de La Cruz, Macromolecules **37**, 9231 (2004).
[37]A. V. Ermoshkin and M. Olvera de La Cruz, Macromolecules **36**, 7824 (2003).
[38]M. Castelnovo and J.-F. Joanny, Langmuir **16**, 7524 (2000).
[39]K. T. Delaney and G. H. Fredrickson, J. Chem. Phys. **146**, 224902 (2017).
[40]J. Lee, Y. O. Popov, and G. H. Fredrickson, J. Chem. Phys. **128**, 224908 (2008).
[41]S. L. Perry and C. E. Sing, Macromolecules **48**, 5040 (2015).
[42]J. B. Schlenoff, A. H. Rmaile, and C. B. Bucur, J. Am. Chem. Soc. **130**, 13589 (2008).
[43]T. R. Farhat and J. B. Schlenoff, J. Am. Chem. Soc. **125**, 4627 (2003).
[44]G. S. Manning, J. Chem. Phys. **51**, 924 (1969).
[45]R. J. Nap, S. H. Park, and I. Szleifer, J. Polym. Sci., Part B: Polym. Phys. **52**, 1689 (2014).
[46]P. Gong, J. Genzer, and I. Szleifer, Phys. Rev. Lett. **98**, 018302 (2007).
[47]M. Tagliazucchi, M. Olvera de la Cruz, and I. Szleifer, Proc. Natl. Acad. Sci. U. S. A. **107**, 5300 (2010).
[48]G. Zaldivar and M. Tagliazucchi, ACS Macro Lett. **5**, 862 (2016).
[49]A. N. Semenov and M. Rubinstein, Macromolecules **31**, 1373 (1998).
[50]R. Nap, P. Gong, and I. Szleifer, J. Polym. Sci., Part B: Polym. Phys. **44**, 2638 (2006).
[51]R. J. Nap, S. H. Park, and I. Szleifer, Soft Matter **14**, 2365 (2018).
[52]M. Tagliazucchi, X. Li, M. Olvera De La Cruz, and I. Szleifer, ACS Nano **8**, 9998 (2014).
[53]A. M. Rumyantsev, E. Y. Kramarenko, and O. V. Borisov, Macromolecules **51**, 6587 (2018).
[54]I. Szleifer and M. A. Carignano, Adv. Chem. Phys. **94**, 165 (1996).
[55]M. Rubinstein and R. H. Colby, *Polymer Physics* (Oxford University Press, New York, 2003).
[56]P. Pincus, Macromolecules **24**, 2912 (1991).
[57]M. A. Carignano and I. Szleifer, Macromolecules **27**, 702 (1994).
[58]J. G. Eberhart, J. Chem. Educ. **87**, 331 (2010).
[59]J. Yu, N. E. Jackson, X. Xu, B. K. Brettmann, M. Ruths, J. J. de Pablo, and M. Tirrell, Sci. Adv. **3**, eaao1497 (2017).
[60]B. W. Ninham and V. A. Parsegian, J. Theor. Biol. **31**, 405 (1971).
[61]C. J. Fennell, A. Bizjak, V. Vlachy, and K. A. Dill, J. Phys. Chem. B **113**, 6782 (2009).
[62]B. Zhao and T. He, Macromolecules **36**, 8599 (2003).
[63]B. Zhao, R. T. Haasch, and S. MacLaren, J. Am. Chem. Soc. **126**, 6124 (2004).